Catalysis Today 265 (2016) 14–18

Contents lists available at ScienceDirect

Catalysis Today

journal homepage: www.elsevier.com/locate/cattod

Titanium-promoted Au–Ti bimetallic nanoparticle catalysts for CO oxidation: A theoretical approach

Kihoon Bang, Kihyun Shin, Myung Shin Ryu, Soonho Kwon, Hyuck Mo Lee*

Department of Material Science and Engineering, KAIST, 291 Daehak-ro, Yuseong-gu, Daejeon 305-701, Republic of Korea

ARTICLE INFO

Article history:
Received 30 June 2015
Received in revised form 24 August 2015
Accepted 1 September 2015
Available online 3 November 2015

Keywords:
CO oxidation
Supported Au–Ti bimetallic nanoparticle
Density functional thoery
Reaction barrier

ABSTRACT

To solve the problems of deactivation of Au nanoparticle (NP) catalysts, we studied the catalytic activity of 10-atom Au–Ti bimetallic NPs on TiO_2 (1 1 0) supports for CO oxidation by means of density function theory (DFT) calculation with DFT + U method. The calculations showed that Au–Ti NPs were more strongly adsorbed on TiO_2 than Au monometallic NPs. The adsorption energy of O_2 was higher on Au–Ti NPs than on Au NPs, leading to low CO poisoning. The reaction barrier for CO oxidation reaction at interfacial site was lower in the Au–Ti NP system. These results suggest that Au–Ti NPs are a promising catalyst for CO oxidation.

1. Introduction

Unlike inert property of bulk gold, gold nanoparticles (NPs) with size of a few nanometers supported on metal oxide (MO_x) supports show high catalytic activity for the oxidation of small molecules such as CO, even at temperatures below room temperature [1,2]. Since the discovery of the high catalytic activity of gold NPs, numerous studies have been performed to explain this high catalytic activity of gold NPs [3–8]. Although it has not yet fully understood, the interaction between NPs and MO_x is thought to be one of the key factors in the catalytic activity of gold NPs [7,9].

However, the gold NP/MO_x catalyst system has several critical problems that prevent its use as catalysts in CO oxidation. One of these problems is deactivation. The active sites of the system are easily poisoned by CO because of the relatively high adsorption energy of CO than of O_2 [10]. Furthermore, the weak interaction between NP and MO_x supports leads to the agglomeration or detachment of NPs [11]. Both phenomena decrease the activity of the catalyst. In addition, the cost for Au NP catalyst is quite high; Au is as expensive as other noble metals such as Pt, Pd, and Ag.

One way to solve the above mentioned problems is to use bimetallic catalysts [12–15]. Here, we propose the use of Au–Ti bimetallic NPs on a TiO_2 support. We chose Ti as the bimetallic component for the following reasons. First, bimetallic Ti–Pt NP catalysts showed low CO adsorption energy [16,17], which is the main factor in CO poisoning. In addition Ti is more abundant and cheaper than Au. Thus, Au–Ti bimetallic catalysts would be less costly than Au monometallic catalysts.

In this report, we studied the catalytic activity of Au–Ti NP on TiO_2 support system for CO oxidation using density functional theory (DFT) calculations to establish whether the Au–Ti NPs are an applicable catalysts for CO oxidation catalysts. In Section 3.1, we performed DFT calculations on various structures of the NP/TiO_2 system and obtained the most stable structure. Using the final structure, we evaluated the adsorption properties of CO and O_2 molecules for CO oxidation in Section 3.2. Finally, we calculated the energy barrier of the reaction in Section 3.3. As a result, we evaluated the stability and catalytic activity of the Au–Ti bimetallic NP on TiO_2 support.

2. Computational details

Spin-polarized DFT calculations with plane-wave basis sets were carried out using the Vienna Ab initio Simulation package [18–20]. We used the generalized gradient approximation with the PW91 functional to describe the exchange-correlation energy of electrons [21]. Ionic cores were treated by the projector-augmented wave method [21,22]. The plane-wave cut-off was set to 400 eV and the convergence criteria for electronic structure and atomic geometry were 1.0×10^{-4} eV and 0.03 eV/Å, respectively.

To treat the highly localized Ti 3d orbitals, DFT + *U* method of Dudarev et al. [23] was applied. Using the scheme of Lutfalla's [24],

* Corresponding author. Tel.: +82 42 350 3334; fax: +82 42 350 3310.
E-mail address: hmlee@kaist.ac.kr (H.M. Lee).

http://dx.doi.org/10.1016/j.cattod.2015.09.040
0920-5861/

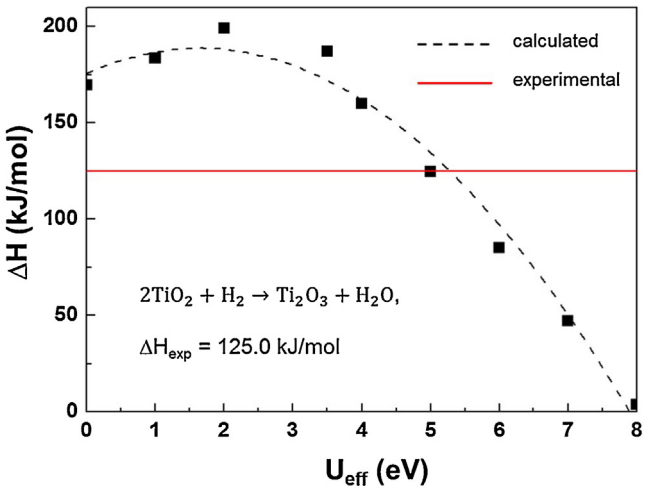

Fig. 1. The effect of U_{eff} on reduction energy of TiO_2 to Ti_2O_3. Black dot is calculated energy, and red line is experimental energy. (For interpretation of the references to color in this figure legend, the reader is referred to the web version of this article.)

the effective U value (U_{eff}) for titanium was calibrated by fitting the energy for the following reduction reaction of rutile TiO_2:

$$2TiO_2 + H_2 \rightarrow Ti_2O_3 + H_2O \quad (1)$$

The rectangular unit cell of bulk rutile TiO_2 is composed of two Ti atoms and four O atoms, and the hexagonal unit cell of Ti_2O_3 is composed of 12 titanium atoms and 18 oxygen atoms. We did geometry optimization and calculated energy for bulk TiO_2 and bulk Ti_2O_3 with a $(4 \times 4 \times 4)$ Monkhorst-Pack grid and a $(2 \times 2 \times 2)$ Γ-centered grid, respectively. The experimental reduction energy, 125 kJ/mol [24], is mostly matched for U_{eff} = 5.0 eV, as shown in Fig. 1. This value was used as the optimal U_{eff} value in later calculations.

To study catalytic properties, a rutile TiO_2 (1 1 0) support was modeled by a (4×2) surface unit cell with three tri-layers (O–Ti–O) and 20 Å of vacuum layers as shown in Fig. 2(a and b). The upper two tri-layers were fully relaxed by geometry optimization. Metal NP was prepared on the TiO_2 surface using 10 atoms of Au and Ti: Au_{10}, Au_9Ti_1, Au_8Ti_2, and Au_7Ti_3. A $(2 \times 2 \times 1)$ Monkhorst-Pack grid k-point sampling was used to calculate the total energies of the systems.

The adsorption energy (E_{ads}) of adsorbate A on adsorbent B was calculated by following equation:

$$E_{ads} = E_{A-B} - E_A - E_B \quad (2)$$

where E_{A-B} is the total energy of the system where A is adsorbed on B, and E_A and E_B are the total energies of A and B each. The transition states (TS) of a CO oxidation reaction were determined with the climbing image nudged elastic band method [25,26].

3. Results and discussion

3.1. Structural stability and electric properties of Au–Ti NPs on TiO_2 support

To identify the stable structures of Au and Au–Ti NPs, we first attached various Au_{10} NP structures on TiO_2 support and relaxed using geometry optimization. We have tested pyramid-like, hemisphere-like, and cage-like initial structures, and the most stable structure was found to be the cage-like structure (Figs. Fig. 2 and 3(a)). From the stable Au_{10} structure, we substituted one of the Au atoms with Ti and again relaxed the structure to obtain the stable Au_9Ti_1 NP structure. The structures of Au_8Ti_2 and Au_7Ti_3 NPs were obtained in a similar fashion. The resulting structures were also cage-like structure, similar to that of the Au_{10} NP (Fig. 3(c and d)). For Au_9Ti_1 NPs, the substitution of Au with Ti in the second and third layers was more unstable than the substitution in the first layer by 1.57 eV and 3.14 eV, respectively. It implies that Ti tends to be close to TiO_2 and interacts strongly with it.

The tendency of interaction can be also seen from the adsorption energy of NPs on the TiO_2 support, as plotted in Fig. 3(b). As the number of Ti atoms in the NP increased, the adsorption energy of the NP became stronger due to the large interaction between Ti and TiO_2. These strong adsorption energies of Au–Ti bimetallic NPs would reduce the degrees of sintering or detachment of NPs from the support [27,28]; thus, Au–Ti NPs would have higher stability than Au monometallic NPs.

We performed Bader charge analysis [28,29] for metal NPs and TiO_2 support (Table 1). The upper two layers of bare TiO_2 support

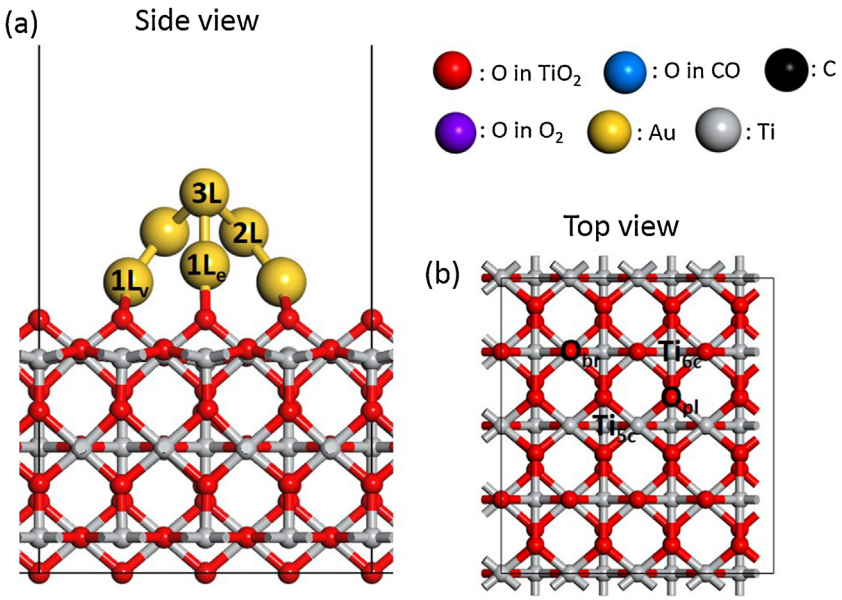

Fig. 2. (a) Side view of our cage-like NP/TiO_2 model and (b) top view of TiO_2 (1 1 0) support. $1L_v$, $1L_e$, 2L, and 3L denote Au atom of 1st layer vertex, 1st layer edge site, 2nd layer, and 3rd layer in metal NP, respectively. Ti_{5c}, Ti_{6c}, O_{br}, and O_{pl} denote fivefold coordinated Ti, sixfold coordinated Ti, bridging O, and in-plane O, respectively.

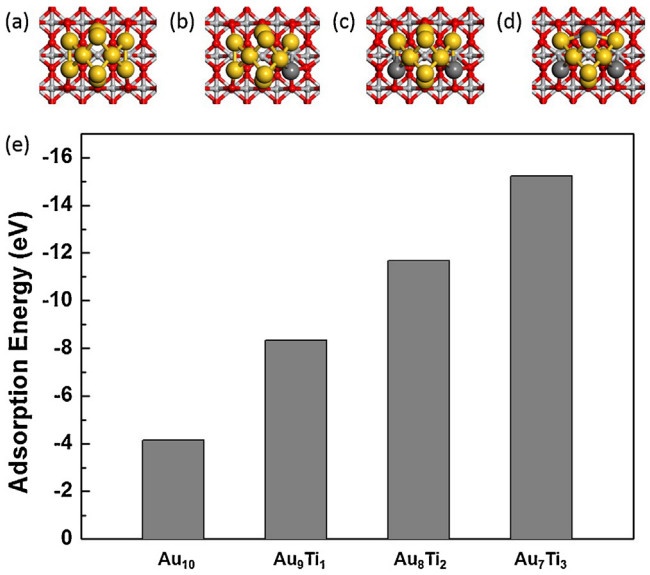

Fig. 3. Stable structure of (a) Au_{10}, and (b) Au_9Ti_1, (c) Au_8Ti_2, (d) Au_7Ti_3. (e) The adsorption energy of each NP on TiO_2 support.

Table 1
Average Bader charges of Au atoms in each layer of metal NP and upper two layers in TiO_2 support. The unit is elementary charge (e^-).

	Au 1L	Au 2L	Au 3L	TiO_2
Au_{10}	0.153	0.053	−0.050	−0.004
Au_9Ti_1	0.120	−0.101	−0.069	−0.017
Au_8Ti_2	0.046	−0.223	−0.082	−0.021
Au_7Ti_3	−0.067	−0.321	−0.210	−0.028

is partially oxidized (+0.005e^- on average) before the adsorption of metal NPs. When we attached Au and Au–Ti NPs to the support, the electrons were partially transferred from the metal NPs to upper two layers of TiO_2 support, because of the reducibility of TiO_2. As the metal NPs changed from Au monometallic to Au–Ti bimetallic NPs, the TiO_2 support and the Au atoms became more negatively charged owing to the charge-transfer from Ti atoms in metal NPs. This large charge transfer would result from the large electronegativity difference between Ti (1.54) and Au (2.54) [30].

3.2. Adsorption properties of CO and O_2 on the Au–Ti/TiO_2 system

The adsorptions of CO and O_2 are a necessary step for CO the oxidation reaction to occur. However, overly strong adsorption of CO leads to the poisoning of catalysts. Therefore, we calculated the adsorption properties of CO and O_2 on the Au and Au–Ti NPs on TiO_2 support for various adsorption sites on the NPs and support. The stable adsorption sites are shown in Fig. 4. CO and O_2 were strongly adsorbed on Au atoms on the third layer (Fig. 4(a, b and d)), Au atoms on the edge of first layer (Fig. 4(b)), and five-coordinated Ti atoms on TiO_2 support (Fig. 4(c and f)). These atoms have low coordination number compared to other atoms; thus, small molecules would be adsorbed more strongly on these low-coordinated atoms [31].

CO is usually strongly adsorbed on metal NPs via backbonding between CO and the metal atom [32]. In the present system, the adsorption energies of CO on metal NPs (see Fig. 4(d and e)) were also very high: −1.03, −1.07, −1.10, and −1.14 eV for Au_{10}, Au_9Ti_1, Au_8Ti_2, and Au_7Ti_3 NPs, respectively, as shown by black and red dots in Fig. 5(a). However, the adsorption on support (see Fig. 4(f)) is quite weaker than the adsorption on NPs. In addition, as metal NPs were attached and changed from Au NP to Au–Ti NPs, the adsorption energies were reduced from −0.49 eV for bare TiO_2 to −0.37, −0.30, −0.31, and −0.30 eV for Au_{10}, Au_9Ti_1, Au_8Ti_2, and Au_7Ti_3 NPs, respectively, as shown by blue dots in Fig. 5(a). The effect is explained by the charge of the support. As shown in Table 1, the upper two layers of the TiO_2 support became negatively charged when metal NPs were attached and the number of Ti atoms in the metal NP increased. Because CO is a strong reducing agent, it prefers to bind to more positive surfaces.

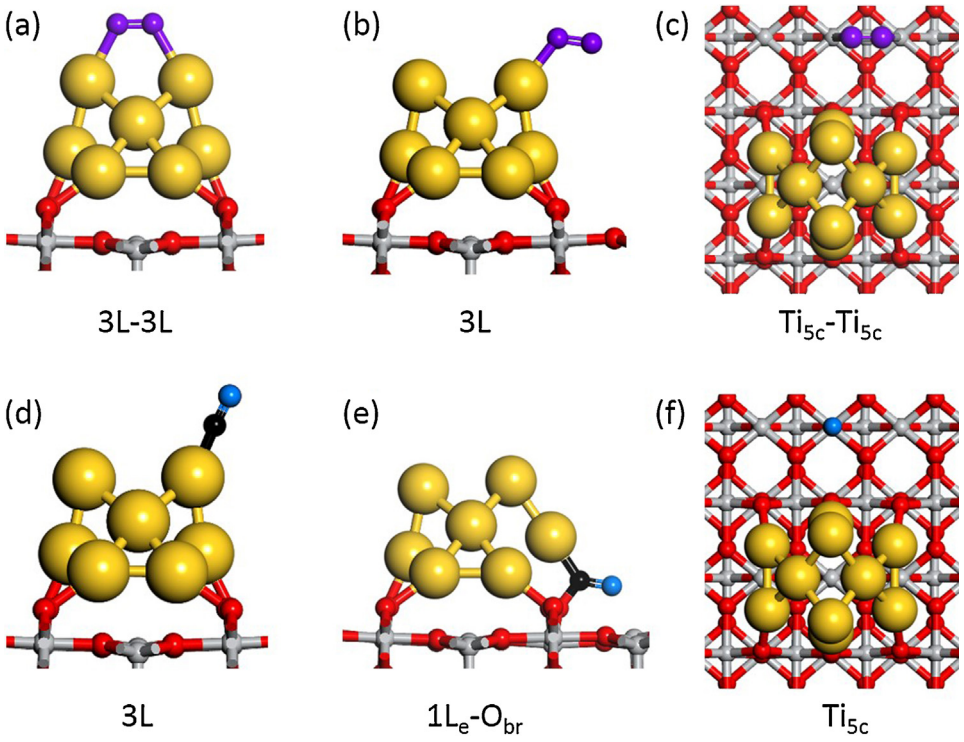

Fig. 4. The stable adsorption site of (a–c) O_2 and (d–f) CO on NP/TiO_2 model. (a–b), (d–e) site is adsorption on NP and (d), (f) site is adsorption on TiO_2 support.

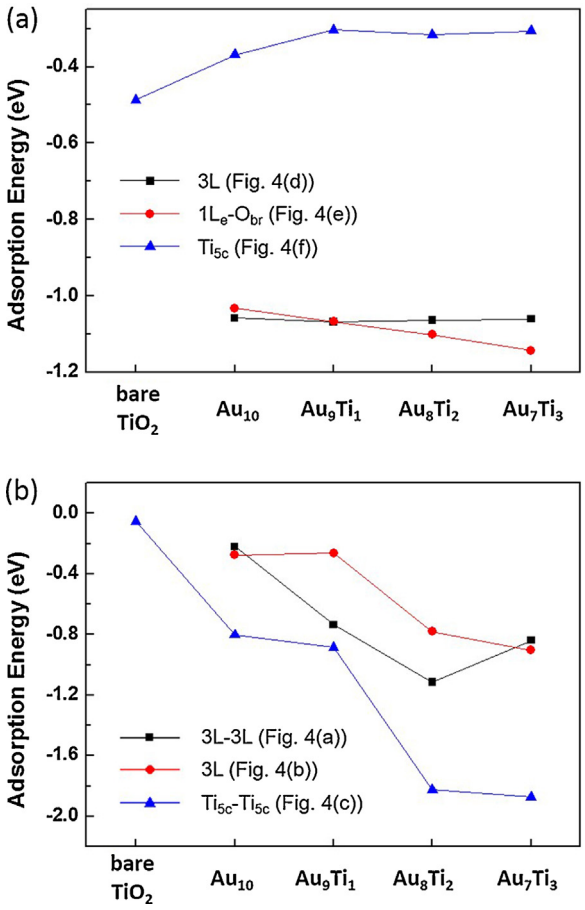

Fig. 5. The adsorption energy of (a) CO and (b) O_2 on NP/TiO_2 model. Black and red dots denote the adsorption on NP, and blue dots denote the adsorption on TiO_2 support. (For interpretation of the references to color in this figure legend, the reader is referred to the web version of this article.)

The adsorption energy of O_2 on metal NPs (see Fig. 4(a and b)) is shown by black and red dots in Fig. 5(b). The adsorption energy of O_2 on Au_{10} monometallic NP is quite low (−0.22 and −0.28 eV), as reported in other studies [4,12]; it is approximately 0.75 eV lower than the adsorption energy of CO. This difference in adsorption energy between O_2 and CO would hinder the adsorption of O_2 and lead to CO poisoning on metal NPs, reducing the activities of metal NP catalysts. However, the adsorption energies of O_2 on metal NPs were much higher for the Au–Ti bimetallic NP systems. The adsorption energies were −0.73, −1.12, and −0.90 eV for Au_9Ti_1, Au_8Ti_2, and Au_7Ti_3 NPs, respectively. Compared to the adsorption energies of CO on Au–Ti NPs, the differences in adsorption energy were 0.33, −0.01, and 0.23 eV for Au_9Ti_1, Au_8Ti_2, and Au_7Ti_3 NPs, respectively. These differences were much lowered than the adsorption energy gap for Au_{10} monometallic NP, and they even became negative for Au_8Ti_2 NPs. This lower adsorption energy gap would allow the O_2 to compete to adsorb on the metal NPs and reduce CO poisoning.

If no metal NPs are present on the support, the adsorption energy of O_2 on the TiO_2 support is very low (−0.05 eV). However, with the Au and Au–Ti NPs are attached (see Fig. 4(c)), the adsorption energies increased considerably to −0.80, −0.88, −1.83, and −1.87 eV for Au_{10}, Au_9Ti_1, Au_8Ti_2, and Au_7Ti_3 NPs, respectively, as shown by blue dots in Fig. 5(b). These energies are even larger than the adsorption energies of CO on the TiO_2 support, unlike the adsorption energies on metal NPs. These adsorption energy differences would suppress CO adsorption and CO support on the TiO_2 support. In addition, the high adsorption energies of O_2 on the TiO_2 support for Au–Ti bimetallic NP systems would allow the support

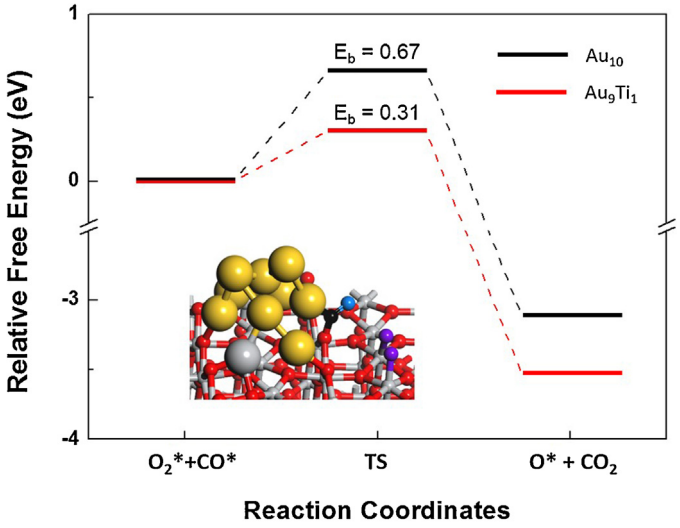

Fig. 6. Energy profile diagram of CO oxidation reaction at the interfacial site of Au_{10} and Au_9Ti on TiO_2 support. Asterisk (*) means adsorbed molecules. The inset refers to the optimized transition state structure of CO oxidation reaction of Au_9Ti_1 NP systems.

to supply O_2 to NP catalysts for the CO oxidation; thus, we could expect high CO oxidation rates at the interfacial sites between NP and the TiO_2 support [4].

3.3. CO oxidation at interfacial site between Au–Ti NPs and TiO_2 support

The CO oxidation reaction has been reported to occur predominantly at the interfacial site between Au NPs and the TiO_2 support [4,7,9]. In our Au and Au–Ti NP systems, CO strongly adsorbs on metal NPs and O_2 strongly adsorbs on the TiO_2 support as shown in Section 3.2; thus, we expect that the interfacial site to be the most probable reaction site for CO oxidation reaction, where CO is provided by NPs and O_2 by the support. Also the reaction barrier at the interfacial site of Au_{10} NP is about 0.40 eV lower than the reaction on the top of Au_{10} NPs. Therefore, we further studied the CO oxidation reaction at this interfacial site and compared two NPs: Au_{10} and Au_9Ti_1.

We set the initial state as CO adsorbed on edge site (Fig. 4(e)) and O_2 on Ti_{5c}–Ti_{5c} bridging site (Fig. 4(c)) because this coadsorption geometry has the highest adsorption energy. The energy profile diagrams of CO oxidation reaction from this initial state for Au_{10} and Au_9Ti_1 NP systems are shown in Fig. 6. The calculated reaction barrier for the Au_{10} NP system was 0.67 eV. In contrast, the reaction barrier for the Au_9Ti_1 NP system was lowered to 0.31 eV. This low reaction barrier for the Au_9Ti_1 NP system related to the high adsorption energy of O_2 on the TiO_2 support. The inset of Fig. 6 shows that the transition state is related to the dissociation of O_2 adsorbed on the TiO_2 support. When the adsorption energy of O_2 becomes higher, adsorbed O_2 is more easily dissociated [33,34], lowering the reaction barrier for the CO oxidation reaction. This low reaction barrier indicates that the Au_9Ti_1 NPs system would have a higher CO oxidation rate than the Au monometallic NPs.

4. Conclusion

Herein, we have investigated the catalytic activity of Au–Ti NPs for CO oxidation using DFT calculations. The U_{eff} value of the DFT + U method was calibrated using the experimental reduction energy of TiO_2 and was found to be 5.0 eV for the PW91 functional. The stable structures of Au monometallic and Au–Ti bimetallic NPs on TiO_2

support were both cage-like structures. The electrons of Ti atoms in the Au–Ti NPs were transferred to the Au atoms and the TiO_2 support surface. As the NP and support became more negatively charged than the Au monometallic NP system, the adsorption energies of O_2 increased on both the NPs and the support. This implies that the CO oxidation at interfacial site between the support and the NPs, where CO is provided by NP and O_2 by support, would be more active in the Au–Ti bimetallic NP system. The calculated reaction barrier was lower for the Au–Ti bimetallic NP system. The result of this work suggest that that Au–Ti NP is more effective catalyst than Au-only NPs.

Acknowledgments

This research was supported by the National Research Foundation of Korea (NRF) grant funded by the Ministry of Science, ICT & Future Planning (MSIP) (NO. NRF-2015R1A5A1037627) and the NLRL (National Leading Research Laboratory) program by the Korea government (MEST) (no. 2011-0028612).

References

[1] M. Haruta, T. Kobayashi, H. Sano, N. Yamada, Novel gold catalysts for the oxidation of carbon monoxide at a temperature far below 0 °C, Chem. Lett. 16 (1987) 405–408.
[2] M. Haruta, Size- and support-dependency in the catalysis of gold, Catal. Today 36 (1997) 153–166.
[3] H.Y. Kim, H.M. Lee, G. Henkelman, CO oxidation mechanism on CeO_2-supported Au nanoparticles, J. Am. Chem. Soc. 134 (2012) 1560–1570.
[4] L. Li, Y. Gao, H. Li, Y. Zhao, Y. Pei, Z. Chen, X.C. Zeng, CO oxidation on TiO_2 (1 1 0) supported subnanometer gold clusters: size and shape effects, J. Am. Chem. Soc. 135 (2013) 19336–19346.
[5] Q. Fu, H. Saltsburg, M. Flytzani-Stephanopoulos, Active nonmetallic Au and Pt species on ceria-based water–gas shift catalysts, Science 301 (2003) 935–938.
[6] M. Haruta, When gold is not noble: catalysis by nanoparticles, Chem. Rec. 3 (2003) 75–87.
[7] I.X. Green, W. Tang, M. Neurock, J.T. Yates, Spectroscopic observation of dual catalytic sites during oxidation of CO on a Au/TiO_2 catalyst, Science 333 (2011) 736–739.
[8] J. Saavedra, H.A. Doan, C.J. Pursell, L.C. Grabow, B.D. Chandler, The critical role of water at the gold–titania interface in catalytic CO oxidation, Science 345 (2014) 1599–1602.
[9] H. Koga, K. Tada, M. Okumura, DFT study of CO oxidation over Au/TiO_2(1 1 0): the extent of the reactive perimeter zone, Chem. Phys. Lett. 610 (2014) 76–81.
[10] A.U. Nilekar, S. Alayoglu, B. Eichhorn, M. Mavrikakis, Preferential CO oxidation in hydrogen: reactivity of core–shell nanoparticles, J. Am. Chem. Soc. 132 (2010) 7418–7428.
[11] P. Konova, A. Naydenov, C. Venkov, D. Mehandjiev, D. Andreeva, T. Tabakova, Activity and deactivation of Au/TiO_2 catalyst in CO oxidation, J. Mol. Catal. A: Chem. 213 (2004) 235–240.
[12] Q. Cai, X. Wang, J.-g. Wang, Distinctions between supported Au and Pt catalysts for CO oxidation: insights from DFT study, J. Phys. Chem. C 117 (2013) 21331–21336.
[13] L. Zhang, H.Y. Kim, G. Henkelman, CO oxidation at the Au–Cu interface of bimetallic nanoclusters supported on CeO_2(1 1 1), J. Phys. Chem. Lett. 4 (2013) 2943–2947.
[14] J.Y. Park, Y. Zhang, S.H. Joo, Y. Jung, G.A. Somorjai, Size effect of RhPt bimetallic nanoparticles in catalytic activity of CO oxidation: role of surface segregation, Catal. Today 181 (2012) 133–137.
[15] N.R. Kim, K. Shin, I. Jung, M. Shim, H.M. Lee, Ag–Cu bimetallic nanoparticles with enhanced resistance to oxidation: a combined experimental and theoretical study, J. Phys. Chem. C 118 (2014) 26324–26331.
[16] H. Abe, F. Matsumoto, L.R. Alden, S.C. Warren, H.D. Abruña, F.J. DiSalvo, Electrocatalytic performance of fuel oxidation by Pt3Ti nanoparticles, J. Am. Chem. Soc. 130 (2008) 5452–5458.
[17] P.C. Jennings, B.G. Pollet, R.L. Johnston, Theoretical studies of Pt–Ti nanoparticles for potential use as PEMFC electrocatalysts, Phys. Chem. Chem. Phys. 14 (2012) 3134–3139.
[18] G. Kresse, J. Furthmüller, Efficiency of ab-initio total energy calculations for metals and semiconductors using a plane-wave basis set, Comput. Mater. Sci. 6 (1996) 15–50.
[19] G. Kresse, J. Hafner, *Ab initio* molecular dynamics for liquid metals, Phys. Rev. B: Condens. Matter 47 (1993) 558–561.
[20] G. Kresse, J. Hafner, *Ab initio* molecular-dynamics simulation of the liquid-metal—amorphous-semiconductor transition in germanium, Phys. Rev. B: Condens. Matter 49 (1994) 14251–14269.
[21] J.P. Perdew, Y. Wang, Accurate and simple analytic representation of the electron–gas correlation energy, Phys. Rev. B: Condens. Matter 45 (1992) 13244–13249.
[22] G. Kresse, D. Joubert, From ultrasoft pseudopotentials to the projector augmented-wave method, Phys. Rev. B: Condens. Matter 59 (1999) 1758–1775.
[23] S.L. Dudarev, G.A. Botton, S.Y. Savrasov, C.J. Humphreys, A.P. Sutton, Electron-energy-loss spectra and the structural stability of nickel oxide: an LSDA+U study, Phys. Rev. B: Condens. Matter 57 (1998) 1505–1509.
[24] S. Lutfalla, V. Shapovalov, A.T. Bell, Calibration of the DFT/GGA+U method for determination of reduction energies for transition and rare earth metal oxides of Ti, V, Mo, and Ce, J. Chem. Theory Comput. 7 (2011) 2218–2223.
[25] G. Henkelman, B.P. Uberuaga, H. Jónsson, A climbing image nudged elastic band method for finding saddle points and minimum energy paths, J. Chem. Phys. 113 (2000) 9901–9904.
[26] G. Henkelman, H. Jónsson, Improved tangent estimate in the nudged elastic band method for finding minimum energy paths and saddle points, J. Chem. Phys. 113 (2000) 9978–9985.
[27] J.A. Farmer, C.T. Campbell, Ceria maintains smaller metal catalyst particles by strong metal-support bonding, Science 329 (2010) 933–936.
[28] G. Henkelman, A. Arnaldsson, H. Jónsson, A fast and robust algorithm for Bader decomposition of charge density, Comput. Mater. Sci. 36 (2006) 354–360.
[29] W. Tang, E. Sanville, G. Henkelman, A grid-based Bader analysis algorithm without lattice bias, J. Phys.: Condens. Matter 21 (2009) 084204.
[30] A.L. Allred, Electronegativity values from thermochemical data, J. Inorg. Nucl. Chem. 17 (1961) 215–221.
[31] S.C. Carabineiro, B. Nieuwenhuys, Adsorption of small molecules on gold single crystal surfaces, Gold Bull. 42 (2009) 288–301.
[32] S.S. Sung, R. Hoffmann, How carbon monoxide bonds to metal surfaces, J. Am. Chem. Soc. 107 (1985) 578–584.
[33] M.D. Rasmussen, L.M. Molina, B. Hammer, Adsorption, diffusion, and dissociation of molecular oxygen at defected TiO_2(1 1 0): a density functional theory study, J. Chem. Phys. 120 (2004) 988–997.
[34] L. Liu, Q. Liu, Y. Zheng, Z. Wang, C. Pan, W. Xiao, O_2 adsorption and dissociation on a hydrogenated anatase (1 0 1) surface, J. Phys. Chem. C 118 (2014) 3471–3482.